

# Comments on Warm Dark Matter Measurements and Limits

Bruce Hoeneisen 

Universidad San Francisco de Quito, Quito, Ecuador

Email: bhoeneisen@usfq.edu.ec

**How to cite this paper:** Hoeneisen, B. (2022) Comments on Warm Dark Matter Measurements and Limits. *International Journal of Astronomy and Astrophysics*, 12, 94-109. <https://doi.org/10.4236/ijaa.2022.121006>

**Received:** February 10, 2022

**Accepted:** March 15, 2022

**Published:** March 18, 2022

Copyright © 2022 by author(s) and Scientific Research Publishing Inc.

This work is licensed under the Creative Commons Attribution International License (CC BY 4.0).

<http://creativecommons.org/licenses/by/4.0/>



Open Access

## Abstract

Observed spiral galaxy rotation curves allow a measurement of the warm dark matter particle velocity dispersion and mass. The measured thermal relic mass  $m_h \approx 100$  eV is in disagreement with limits, typically in the range 1 to 4 keV. We review the measurements, update the no freeze-in and no freeze-out scenario of warm dark matter, and try to identify the cause of the discrepancies between measurements and limits.

## Keywords

Warm Dark Matter, Spiral Galaxy Rotation Curves, Stellar Mass Distributions, Lyman- $\alpha$  Forest

## 1. Introduction

The  $\Lambda$  cold dark matter ( $\Lambda$ CDM) cosmological model, based on just 6 parameters [1], is in spectacular agreement with precision measurements of the cosmic microwave background anisotropies, the power spectrum of large scale density fluctuations, and baryon acoustic oscillations. The  $\Lambda$ CDM model may have tensions with observations on scales smaller than the Galaxy, e.g. too few satellites of the Milky Way and Andromeda, and galaxies with cores instead of the cusps expected from simulations. An extension of the  $\Lambda$ CDM cosmology that addresses the small scale tensions is  $\Lambda$  warm dark matter ( $\Lambda$ WDM) that assumes that the dark matter has a non-negligible velocity dispersion. Since the non-relativistic velocity dispersion  $v_{\text{hrms}}(a)$  scales as  $a^{-1}$ , we may write, for the homogeneous matter dominated universe,

$$v_{\text{hrms}}(a) = \frac{v_{\text{hrms}}(1)}{a} = v_{\text{hrms}}(1) \left[ \frac{\rho_h(a)}{\Omega_c \rho_{\text{crit}}} \right]^{-1/3}, \quad (1)$$

where  $\rho_h(a)$  is the density of dark matter at expansion parameter  $a$  (nor-

malized to  $a = 1$  at the present time), and  $\Omega_c \rho_{\text{crit}}$  is the mean density of dark matter at the present time (we use the standard notation in cosmology, and astrophysical constants, as in [1]).

Let  $P(k)$  be the comoving power spectrum of linear relative density perturbations in the  $\Lambda$ CDM model after decoupling [2].  $k$  is the comoving wavenumber. The corresponding power spectrum in the  $\Lambda$ WDM cosmology is  $P(k)\tau^2(k)$ , where  $\tau^2(k)$  is a cut-off factor due to warm dark matter free-streaming. The cut-off factor, at time  $t_{\text{eq}}$  when matter begins to dominate, has the approximate form (see figure 5 of [3])

$$\tau^2(k) = \exp(-k^2/k_{\text{fs}}^2). \quad (2)$$

Note that we have defined the free-streaming cut-off wavenumber  $k_{\text{fs}}$  so that  $\tau^2(k_{\text{fs}}) \equiv \exp(-1)$ . We will assume that non-relativistic dark matter carries the non-relativistic Maxwell-Boltzmann momentum distribution (see Section 3 below). Given the adiabatic invariant  $v_{\text{hrms}}(1)$ , the comoving free-streaming cut-off wavenumber at  $t_{\text{eq}}$  is [3]

$$k_{\text{fs}}(t_{\text{eq}}) = \frac{1.455}{\sqrt{2}} \sqrt{\frac{4\pi G \bar{\rho}_m(1) a_{\text{eq}}}{v_{\text{hrms}}(1)^2}} = \frac{1.455}{\sqrt{6}} k_J(t_{\text{eq}}). \quad (3)$$

$k_J(t_{\text{eq}})$  is the comoving Jeans wavenumber at matter-radiation equality. This solution corresponds to adiabatic, *i.e.* thermal, initial fluctuations. After  $t_{\text{eq}}$ ,  $M_J \propto a^{-3/2}$  decreases allowing non-linear regeneration of small scale structure. An alternative  $k_{\text{fs}}$ , obtained from simulations, is given in [4].

In summary, the  $\Lambda$ WDM extension of the  $\Lambda$ CDM model adds one parameter: the velocity dispersion  $v_{\text{hrms}}(1)$ . Note that a typical dark matter particle becomes non-relativistic at expansion parameter  $a \approx a'_{\text{hNR}} \equiv v_{\text{hrms}}(1)/c$ . The challenge is to measure, or set limits on,  $v_{\text{hrms}}(1)$  and  $k_{\text{fs}}$ . Measurements of  $k_{\text{fs}}$  need to be done at high redshift  $z$  since non-linear evolution of perturbations regenerate the small scale power spectrum [5] [6] [7].

The warm dark matter extension of the  $\Lambda$ CDM model is not only the addition of a parameter: it is a change of our understanding of the formation of structure [5], galaxy halos [8], first stars, and reionization.

In the present article we briefly review measurements of  $v_{\text{hrms}}(1)$ . These measurements are ruled out by numerous limits. The purpose of this study is to try to understand what went wrong. It turns out that the measurements of the velocity dispersion  $v_{\text{hrms}}(1)$ , and of  $k_{\text{fs}}$ , coincide with the predictions of the no freeze-in and no freeze-out warm dark matter scenario. We also update this scenario.

## 2. Measurements of $v_{\text{hrms}}(1)$

Fits to relaxed spiral galaxy rotation curves allow a measurement of the radial component of the velocity dispersions  $\langle v_{rh}^2 \rangle^{1/2}$  and  $\langle v_{rb}^2 \rangle^{1/2}$ , and the density runs  $\rho_h(r)$  and  $\rho_b(r)$ , of dark matter and baryons, respectively [9]. The velocity

dispersion of dark matter is found to be independent of the radial coordinate  $r$  (out to the radius where the rotation curve remains flat), implying, in particular, that dark matter particles have the non-relativistic Maxwell-Boltzmann momentum distribution (within observational uncertainties) [8] [9]. We define the adiabatic invariant in the core of the galaxy as

$$v_{\text{hms}}(1) \equiv \sqrt{3} \langle v_{rh}^2 \rangle^{1/2} \left( \frac{\Omega_c \rho_{\text{crit}}}{\rho_h(r \rightarrow 0)} \right)^{1/3}. \quad (4)$$

$v_{\text{hms}}(1)$  is the velocity dispersion of dark matter particles that would be obtained by adiabatic expansion from the core of the galaxy to the mean dark matter density of the universe  $\Omega_c \rho_{\text{crit}}$ . The adiabatic invariant  $v_{\text{hms}}(1)$  is predicted to be of cosmological origin, and hence to be equal in all relaxed galaxies [8]. In other words, the velocity dispersion of dark matter in the core of the galaxy with density  $\rho_h(0)$  should be equal to the velocity dispersion of dark matter in the early universe when its density was  $\rho_h(0)$ , since the early universe and the galactic core are connected by adiabatic expansion, turn-around, and adiabatic contraction [8], (see text related to figure 13 of [8] for details). Measurements indicate that “phase space dilution” in relaxed galaxies is not dominant. Therefore we identify  $v_{\text{hms}}(1)$  in Equation (4) with  $v_{\text{hms}}(1)$  in Equation (1). If this identification is correct, then the observed spiral galaxy rotation curves allows a measurement of the temperature-to-mass ratio of dark matter particles

$kT(a)/m_h = v_{\text{hms}}(a)^2/3$ , and also of the free-streaming cut-off wavenumber  $k_{\text{fs}}$ .

Measurements of the adiabatic invariant of 10 relaxed spiral galaxies in the THINGS sample [10] obtains the following mean:

$v_{\text{hms}}(1) = 1.25 \pm 0.10(\text{stat}) \pm 0.75(\text{syst})$  km/s (this uncertainty includes the contribution of the dark matter halo rotation parameter  $\kappa_h = 0.15 \pm 0.15$  km/s) [9].

The measurement of the adiabatic invariant of 40 different galaxies in the SPARC sample [11] obtains the following mean and standard deviation:

$v_{\text{hms}}(1) = \sqrt{1 - \kappa_h} (0.87 \pm 0.27)$  km/s [12]. This result does not depend significantly on the galaxy luminosity over three orders of magnitude, velocity dispersion, gas mass, Vaucouleurs class, disk central surface brightness, or core dark matter density [12]. Estimating  $\kappa_h = 0.15^{+0.35}_{-0.15}$  [9] [13], and including the study of known systematic uncertainties in [13], we obtain

$$v_{\text{hms}}(1) = 0.79 \pm 0.33 (\text{tot}) \text{ km/s}, \quad (5)$$

at 68% confidence.

In summary, the prediction that  $v_{\text{hms}}(1)$  is of cosmological origin, and hence equal in the core of all relaxed galaxies, is validated within the cited uncertainty.

However, the corresponding free-streaming cut-off wavevector

$k_{\text{fs}} = 1.03^{+0.74}_{-0.30} \text{ Mpc}^{-1}$  (from Equation (3)) has been excluded by many studies that obtain lower bounds typically in the range  $8 \text{ Mpc}^{-1}$  to  $38 \text{ Mpc}^{-1}$ , corresponding to thermal relic masses  $m_h$  greater than 1 to 4 keV respectively (with a thermal

relic defined by Equations (6) and (7) of [4]). One purpose of the present study is to try to understand what may have gone wrong.

### 3. The No Freeze-In and No Freeze-Out Scenario

The measured adiabatic invariant  $v_{hrms}$  (1) happens to be in agreement with the following detailed scenario. Dark matter is in thermal and diffusive equilibrium with the Standard Model sector in the early universe, and decouples (from the Standard Model sector and from self-annihilation) while still ultra-relativistic. Elastic dark matter-dark matter interactions are allowed. Thus we assume that dark matter particles decouple with an ultra-relativistic thermal equilibrium (URTE) momentum distribution, either Fermi-Dirac or Bose-Einstein, with zero chemical potential  $\mu$ . Due to the expansion of the universe, dark matter particles become non-relativistic. We assume that the URTE momentum distribution relaxes to the corresponding non-relativistic distribution (NRTE) due to elastic dark matter-dark matter scattering. This latter assumption is needed because only the NRTE is consistent with the flat portion of spiral galaxy rotation curves [8] [9]. Even the quantum repulsion (attraction) between identical fermions (bosons), with a mutual potential

$$\phi(r) = -kT \ln \left[ 1 \mp \exp \left( -m_h kT_h \frac{r^2}{\hbar^2} \right) \right], \quad (6)$$

is sufficient to acquire the NRTE in a very short time scale relative to the age of the universe, assuming quasi-degenerate dark matter [14]. For simplicity, we consider a single dark matter species.

Let  $T_h/T$  be the temperature ratio of dark matter and photons after decoupling of neutrinos, and after  $e^+e^-$  annihilation, and before dark matter becomes non-relativistic. This ratio is

$$\frac{T_h}{T} = \left( \frac{43}{11g_{\text{dec}}} \right)^{1/3}, \quad (7)$$

where  $g_{\text{dec}} = \sum N_b + (7/8) \sum N_f$  at decoupling of dark matter from the Standard Model sector [1].  $N_f$  ( $N_b$ ) is the number of fermion (boson) spin polarizations. As an example, if dark matter couples to the Higgs boson, then it decouples from the Standard Model sector as the temperature drops below  $M_H$  and the Higgs bosons decay. Then  $T_h/T = (43 \times 4 / (11 \times 381))^{1/3} = 0.345$  [1] [15]. We will assume that warm dark matter decouples from the Standard Model sector at a temperature between  $m_t$  and  $T_C$ , where  $T_C$  is the temperature of the confinement-deconfinement transition between quarks and hadrons (decoupling at a lower temperature compromises the agreement with Big Bang Nucleosynthesis). Then  $0.424 > T_h/T > 0.344$ . The ratio of number densities of dark matter particles and photons, after  $e^+e^-$  annihilation until the present time, is

$$\frac{n_h}{n_\gamma} = \frac{43g'_h}{22g_{\text{dec}}}, \quad (8)$$

where  $g'_h = N_b + 3N_f/4$  for the dark matter [14]. Then, at the present time,

$$\Omega_c h^2 = \frac{n_h m_h h^2}{\rho_{\text{crit}}} \approx \frac{114}{g_{\text{dec}}} \frac{g'_h}{1.5 \text{ keV}} m_h \tag{9}$$

determines the dark matter particle mass corresponding to no freeze-in and no freeze-out.

The expansion of dark matter, and the transition from the URTE momentum distribution to the NRTE momentum distribution, is assumed to occur with constant number of particles, *i.e.* the particle number density scales as  $a^{-3}$ , and (arguably) with constant entropy, see [14] for full details. For example, the number density of dark matter particles is calculated as follows:

$$n_h(T_h, \mu) = \frac{4\pi g}{h^3} \int_0^\infty \frac{p^2}{\exp((\varepsilon - \mu)/kT_h) \pm 1} dp, \tag{10}$$

where the particle energy is  $\varepsilon = \sqrt{p^2 c^2 + m_h^2 c^4} - m_h c^2$ , and  $g = N_f$  for dark matter fermions, or  $g = N_b$  for dark matter bosons. Similar equations obtain  $\varepsilon(T_h, \mu)$ , the pressure  $P(T_h, \mu)$ , the root-mean-square velocity  $v_{\text{hrms}}(T_h, \mu)$ , and the dimensionless entropy per particle  $s/k$  [14]. We note that these equations are valid for the entire range of  $T_h$ , from non-relativistic  $kT_h \ll m_h c^2$  to ultra-relativistic  $kT_h \gg m_h c^2$ . This scenario implies that dark matter has a dimensionless entropy per particle:  $s/k = 4.202$  for fermions, and  $s/k = 3.601$  for bosons, and that non-relativistic dark matter acquires a negative chemical potential  $\mu$  [14]. For  $m_h = 1000 \text{ eV}$  (108 eV),  $\mu' \equiv \mu/kT_h = -1.618$  (-1.618) for non-relativistic fermions, and  $\mu' = -1.243$  (-1.243) for non-relativistic bosons. For fermions, from equation (26) of [14], we obtain

$$m_h = 108 \left( \frac{0.76 \text{ km/s}}{v_{\text{hrms}}(1)} \right)^{3/4} \left( \frac{2}{N_f} \right)^{1/4} \text{ eV}, \tag{11}$$

$$\frac{T_h}{T} = 0.336 \left( \frac{v_{\text{hrms}}(1)}{0.76 \text{ km/s}} \right)^{1/4} \left( \frac{2}{N_f} \right)^{1/4}, \tag{12}$$

where  $T_h/T$  is the dark matter-to-photon temperature ratio after  $e^+e^-$  annihilation, and before dark matter becomes non-relativistic. Equation (12) is obtained from (11), (7) and (9). For bosons, from Equation (28) of [14], we obtain

$$m_h = 108 \left( \frac{0.76 \text{ km/s}}{v_{\text{hrms}}(1)} \right)^{3/4} \left( \frac{1}{N_b} \right)^{1/4} \text{ eV}, \tag{13}$$

$$\frac{T_h}{T} = 0.385 \left( \frac{v_{\text{hrms}}(1)}{0.76 \text{ km/s}} \right)^{1/4} \left( \frac{1}{N_b} \right)^{1/4}. \tag{14}$$

Note that the measurement of the adiabatic invariant  $v_{\text{hrms}}(1)$  allows a determination of the dark matter particle mass  $m_h$ , and of the ratio  $T_h/T$  (that determines the dark matter decoupling temperature, if sufficiently precise).

**Table 1** presents a summary of measurements and predictions. The agreement is noteworthy since it depends on the measured values of  $v_{\text{hrms}}(1)$ ,  $k_{\text{fs}}$ ,

**Table 1.** Summary of measurements of the adiabatic invariant  $v_{\text{rms}}(1)$  with spiral galaxy rotation curves [12], the free-streaming cut-off wavenumber  $k_{\text{fs}}$  with galaxy stellar mass distributions at  $z = 4.5, 6, 7$  and  $8$  [13], and predictions from the no freeze-in and no freeze-out scenario.  $a'_{\text{hNR}} \equiv v_{\text{rms}}(1)/c$ . After  $e^+e^-$  annihilation, while dark matter is ultra-relativistic,  $0.424 \geq T_h/T \geq \mathbf{0.344}$ , corresponding to decoupling at  $T_c < T_{\text{dec}} < m_t$ .

Observable	$v_{\text{rms}}(1)$ [km/s]	$10^6 a'_{\text{hNR}}$	$k_{\text{fs}}$ [Mpc $^{-1}$ ]	$m_h$ [eV]
Spiral galaxies	$0.79 \pm 0.33$	$2.64 \pm 1.10$	$1.03^{+0.74}_{-0.30}$	
$M_*$ distribution			$0.90^{+0.44}_{-0.40}$	
Fermions spin 1/2				
No freeze-in/-out	1.93 to <b>0.83</b>	6.43 to <b>2.78</b>	0.42 to <b>0.98</b>	54 to <b>101</b>
Bosons				
No fr-in/-out spin 0	1.12 to <b>0.48</b>	3.73 to <b>1.61</b>	0.73 to <b>1.69</b>	81 to <b>152</b>
No fr-in/-out spin 1*	2.24 to <b>0.97</b>	7.46 to <b>3.22</b>	0.36 to <b>0.84</b>	40 to <b>76</b>

\*For spin 1 dark matter the predictions are model dependent [15].

$\Omega_c$  and  $T_0$ . The (arguably) simplest extensions of the Standard Model for the present scenario, that include scalar, vector or spinor warm dark matter particles, are presented in [15].

Comments: Equations (11) to (14) update Equations (15) to (18) of [13] to the present scenario. Reference [13] assumes non-interacting dark matter (except for gravity), does not consider the URTE to NRTE transition, and assumes zero chemical potential for non-relativistic dark matter. **Table 1** updates table 4 of [13]. Note that in **Table 1** we no longer distinguish fermion from boson dark matter because they become indistinguishable (with the current level of precision) due to their negative non-relativistic chemical potential in the present scenario.

#### 4. A New Paradigm

**Table 1** has a big problem. Numerous studies have excluded a dark matter thermal relic mass  $m_h \approx 100$  eV. The lower bounds are typically in the range 1 to 4 keV. These studies may well be correct, in which case we need to understand why the approximately 60 studied relaxed spiral galaxies have the same adiabatic invariant  $v_{\text{rms}}(1)$  (within statistical and systematic uncertainties), and why the measured  $v_{\text{rms}}(1)$ ,  $k_{\text{fs}}$ ,  $\Omega_c$ , and  $T_0$  happen to agree with the no freeze-in and no freeze-out scenario.

The  $\Lambda$ WDM model adds one parameter to  $\Lambda$ CDM, namely the velocity dispersion  $v_{\text{rms}}(1)$ . This addition implies a change in paradigm, *i.e.* a change in the way we understand cosmology. Dark matter no longer has an infinite phase-space density, and hence simulations need to include the velocity dispersion  $v_{\text{rms}}(1)$  [14], in addition to the small scale power suppression factor  $\tau^2(k)$  due to free-streaming. Galaxies may form adiabatically without requiring relaxation or virialization [8]. The galaxy “virialized” mass (usually measured in simu-

lations up to a radius  $r$  corresponding to  $\rho(r) = 200\bar{\rho}$  is an ill-defined concept as the halo radius keeps growing with a velocity  $\sqrt{3\langle v_{rh}^2 \rangle}$ , and the halo mass keeps increasing linearly with time [8]. The well defined mass of a galaxy is the linear mass of the Press-Schechter formalism, since the dimensions of the perturbation grow in proportion to the expansion parameter  $a$ , while the density scales as  $a^{-3}$ , so the linear mass  $M_h$  is independent of  $a$ . All relaxed galaxies have (approximately?) the same measured adiabatic invariant  $v_{hrms}(1)$  in the core. The warmest dark matter consistent with reionization has (arguably)  $v_{hrms}(1) \approx 0.8$  km/s (if the Gaussian window function turns out to be a good approximation, see Section 5). The first galaxies to form have a stellar mass of order  $M_* \approx 10^7 M_\odot$ . Larger galaxies form hierarchically as in the  $\Lambda$ CDM model [16] [17], and smaller galaxies are “stripped-down” during their formation as they loose matter to neighboring galaxies [6]. This may be the main mechanism of the non-linear regeneration of the small scale structure.

In the  $\Lambda$ CDM scenario the first dark matter halos to collapse have arbitrarily small  $M_h$ , and are devoid of a full complement of baryons due to the baryon pressure [2]. The first galaxies in the  $\Lambda$ CDM scenario to have a full complement of baryons, and to produce first stars, have a stellar mass  $M_*$  of order  $10^5 M_\odot$  and form at  $z \approx 20$ . Galaxy evolution proceeds hierarchically. When galaxies with  $M_* \approx 10^7 M_\odot$  form (at  $z \approx 12$ ) then the evolution of  $\Lambda$ CDM meets the evolution of  $\Lambda$ WDM, and both scenarios reach half reionization at approximately the same redshift  $z = 7.7 \pm 0.7$ , and thereafter are difficult to tell apart due to the non-linear regeneration of small scale structure.

### 5. Comments on the Press-Schechter Galaxy Mass Distribution

The derivation of the Press-Schechter galaxy mass distribution [18], and its Sheth-Tormen ellipsoidal collapse extensions [19] [20], are valid for the hierarchical structure formation of the  $\Lambda$ CDM model, and for redshift  $z \gtrsim 4.5$  before saturation sets in. The derivation of the Press-Schechter relation is based on the variance of the linear relative density perturbation on the linear mass scale  $M_h$  at redshift  $z$  [2]:

$$\sigma^2(M_h, z) = \frac{f^2}{(2\pi)^3 (1+z)^2} \int_0^\infty 4\pi k^2 dk P(k) \tau^2(k) W^2(k). \tag{15}$$

$f$  is a correction due to the accelerated expansion of the universe:

$f = 1, 1.252, 1.269$  for  $z = 0, 2, 11$  respectively.  $W(k)$  is a window function.

$f^2 P(k) \tau^2(k) / (1+z)^2$  is the proper power spectrum at redshift  $z$ .

For the  $\Lambda$ CDM model, with  $\tau^2(k) = 1$ , the usual choice of window function is a 3-dimensional top-hat sphere of radius  $r_0$  in coordinate space:

$W(r) = 3/(4\pi r_0^3)$  for  $r \leq r_0$ , and 0 for  $r > r_0$ . Note that  $W(r)$  is normalized so that its integral over 3-dimensional space is 1. The mass of the perturbation is

$$M_h = \frac{4}{3} \pi r_0^3 \bar{\rho}_h \equiv V_W \bar{\rho}_h. \tag{16}$$

The Fourier transform of  $W(r)$  is

$$W(k) \equiv \int W(r) e^{-ik \cdot r} d^3r = \frac{3}{(kr_0)^3} [\sin(kr_0) - kr_0 \cos(kr_0)]. \quad (17)$$

$4\pi k^2 W(k)$  is ill-behaved: it is oscillatory and does not converge, and is not suited for warm dark matter with a cut-off factor  $\tau^2(k)$ .

For warm dark matter, the usual choice of window function, is a sharp cut-off of  $k$  at  $k_0$ , *i.e.*  $W(k)=1$  for  $k \leq k_0$ ,  $W(k)=0$  for  $k > k_0$  [21] [22]. The appropriate linear mass scale is

$$M_h = \frac{4}{3} \pi \left( \frac{c}{k_0} \right)^3 \bar{\rho}_h, \quad (18)$$

where  $c \approx 2.7$  is calibrated with simulations at  $z \approx 0$  [21]. The Fourier transform of  $W(k)$  is

$$W(r) = \frac{1}{2\pi^2 r^3} [\sin(k_0 r) - k_0 r \cos(k_0 r)]. \quad (19)$$

$4\pi r^2 W(r)$  is ill-behaved: it is oscillatory and does not converge, and has an ill defined volume in  $r$ -space.

Another window function that is considered [13] [23] is the Gaussian:

$$W(k) = \exp\left(-\frac{k^2}{2k_0^2}\right), \quad W(r) = \frac{1}{V_W} \exp\left(-\frac{r^2 k_0^2}{2}\right), \quad (20)$$

with

$$V_W \equiv \frac{4}{3} \pi r_0^3 = \frac{(2\pi)^{3/2}}{k_0^3}, \quad M_h = \frac{4}{3} \pi \left( \frac{1.555}{k_0} \right)^3 \bar{\rho}_h. \quad (21)$$

Note that  $r_0 \approx 1.555/k_0$ . The Gaussian window functions  $W(r)$  and  $W(k)$  are well behaved. In [13] and [23] we choose the Gaussian window function because it obtains excellent agreement with stellar mass distributions at  $z = 8, 7, 6, 4.5$  and 3, and so the Press-Schechter formalism with Gaussian window function, and Gaussian  $\tau^2(k)$  as in (2), is a good description of the data. Whether, or not, it is also a good description of warm dark matter is another question.

A comparison of the distributions with Gaussian and sharp- $k$  window functions is presented in **Figure 1**. With the Gaussian window function excellent agreement with the data is obtained, and  $k_{\text{fs}}$  is *measured*:  $k_{\text{fs}} = 0.90_{-0.40}^{+0.44} \text{ Mpc}^{-1}$  [13], see **Table 1**. Using the sharp- $k$  cut-off in several publications results in *limits* on  $k_{\text{fs}}$ , typically  $k_{\text{fs}} \gtrsim 26 \text{ Mpc}^{-1}$ .

The cut-off factor  $\tau^2(k)$  given by (2) and (3) is valid at  $t_{\text{eq}}$ . Free-streaming continues after  $t_{\text{eq}}$ , but is complicated by gravity and by non-linear regeneration of small scale structure by the time of the formation of first galaxies. During their formation, proto-galaxies may loose matter to neighboring galaxies, or break up, and populate the low mass tail [6] [24]. By  $z = 3$  there remains little memory of  $\tau^2(k)$  at  $t_{\text{eq}}$ , see figure 2 of [5]. This regeneration has been described by Equations (13) and (14) of [25], and adds a long tail to  $\tau^2(k)$ .

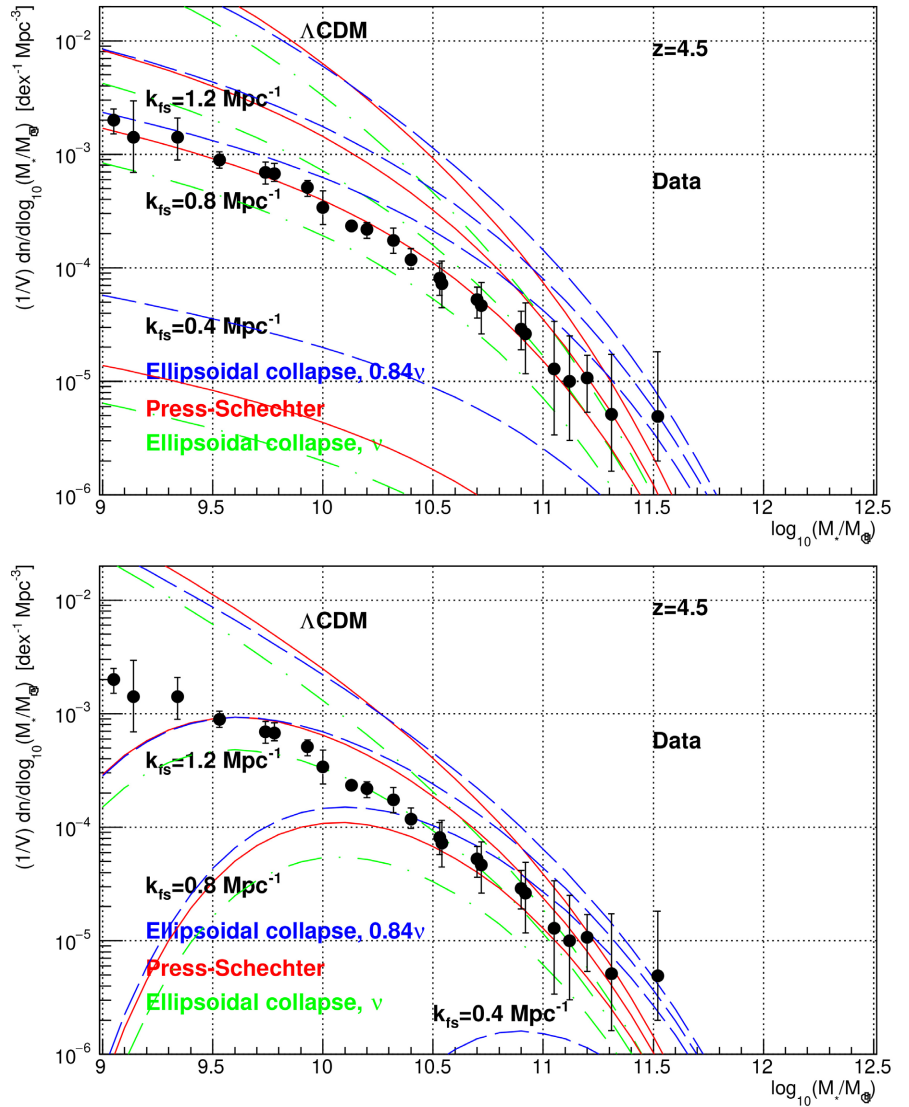


**Figure 1.** Press-Schechter and Sheth-Tormen ellipsoidal collapse predictions of galaxy stellar mass functions are shown (see [23] for details), with Gaussian (top) and sharp- $k$  (bottom) window functions. To match prediction to data at the high mass end we have set  $\log_{10} M_h = \log_{10} M_* + 1.5$  for the Gaussian window function, and  $\log_{10} M_h = \log_{10} M_* + 2.0$  for the sharp- $k$  window function. The top figure is taken from [13] where references to the data are given.

In summary, the discrepancy between the limits and the measurements of  $k_{fs}$  can be traced to the different  $\tau^2(k)$  and window functions used. Additional simulations and studies are needed to settle this issue.

### 6. Simulations

The Press-Schechter formalism with Gaussian window function, describes the observed stellar mass distributions at  $z = 8, 7, 6, 4.5$ , and even 3 [13]. But does it describe warm dark matter? To investigate this question, we generate galaxies with a simple generator described in [16] and [17]. Briefly, we apply periodic

boundary conditions in a cube of comoving side  $L = 300$  Mpc at a given expansion parameter  $a$ , *i.e.* we do not step galaxy evolution in time. We calculate the density  $\rho(\mathbf{x}, I)$  in the linear approximation by summing Fourier terms (with random phases) for comoving wavevectors with  $k < k_I = 2\pi/\lambda_I = 2\pi I/L$ , where  $I$  is an integer. We search for maximums of  $\rho(\mathbf{x}, I)$ . If the maximum exceeds  $2.69\bar{\rho}(a)$  and the proto-galaxy “fits”, we generate a galaxy  $i$  with proper radius  $R_i = a_2\lambda_i/2$ , ( $a_2$  is  $a$  in the linear approximation), and total linear mass  $M_{hi} = (4/3)\pi R_i^3 2.69\bar{\rho}(a)$  (which is different from the often used “virialized” mass). A galaxy “fits” if it does not overlap previously generated galaxies. The integer  $I$  is then increased by 1 and galaxies of a smaller generation are formed. Note that a galaxy that did not fit at generation  $I$  may fit at a “generation” with larger  $I$ , and hence be created with a reduced mass. These are “stripped down” galaxies that have lost matter to neighboring galaxies in the course of their formation [6]. This is a simplified way to regenerate small scale structure in the warm dark matter scenario.

To compare the simulations with data it is necessary to make the transition from the “linear” halo mass  $M_h$  to the stellar mass  $M_*$ . Here we approximate the transformation as a fixed factor, which is adjusted so that data and simulation agree at the high stellar mass end (this factor is very sensitive to the power spectrum normalization  $\Delta_R^2$ ). The results for  $z = 4.5$ , and 6 are presented in **Figure 2**, upper panels. The simulations shown are  $\Lambda$ CDM,  $\Lambda$ WDM with  $k_{fs} = 0.8 \text{ Mpc}^{-1}$ , and the same plus a “tail”:

$$\tau^2(k) = \begin{cases} \exp\left(-\frac{k^2}{k_{fs}^2}\right) & \text{if } k < k_{fs}, \\ \exp\left(-\frac{k}{k_{fs}}\right) & \text{if } k \geq k_{fs}. \end{cases} \quad (22)$$

The bottom left panel of **Figure 2** shows the cut-off factors  $\tau^2(k)$  of (2) and (22), as well as the “linear” cut-off factor (6) and (7) of [4], and the “non-linear” regenerated cut-off factor of (13) and (14) of [25].

An alternative way to estimate the stellar mass is to obtain the galaxy dark matter particle 1-dimensional dispersion velocity as

$$v_{rhms}(\text{gal}) = \frac{v_{\text{flat}}}{\sqrt{2}} = 1.2 \sqrt{2\pi G \bar{\rho}(a)_{\text{gal}} \left( R_i^2 - (\lambda_J(a)/2)^2 \right)}, \quad (23)$$

where the factor  $\approx 1.2$  is calibrated from simulations described in [8], and  $\lambda_J(a)$  is the proper Jeans length. The stellar luminosity in the R band is then obtained from the Tully-Fisher relation [26]

$$\log_{10} \left( \frac{L_R}{L_{\odot}} \right) = 10.5 + 3.5 \log_{10} \left( \frac{v_{\text{flat}}}{200 \text{ km/s}} \right). \quad (24)$$

Finally, to obtain the stellar mass  $M_*/M_{\odot}$  we assume  $M_*/L_* = 0.5M_{\odot}/L_{\odot}$ . The comparison is shown in **Figure 2** bottom right panel.

We conclude that the data are in agreement with the Press-Schechter prediction with the Gaussian window function [13], and are also in agreement with

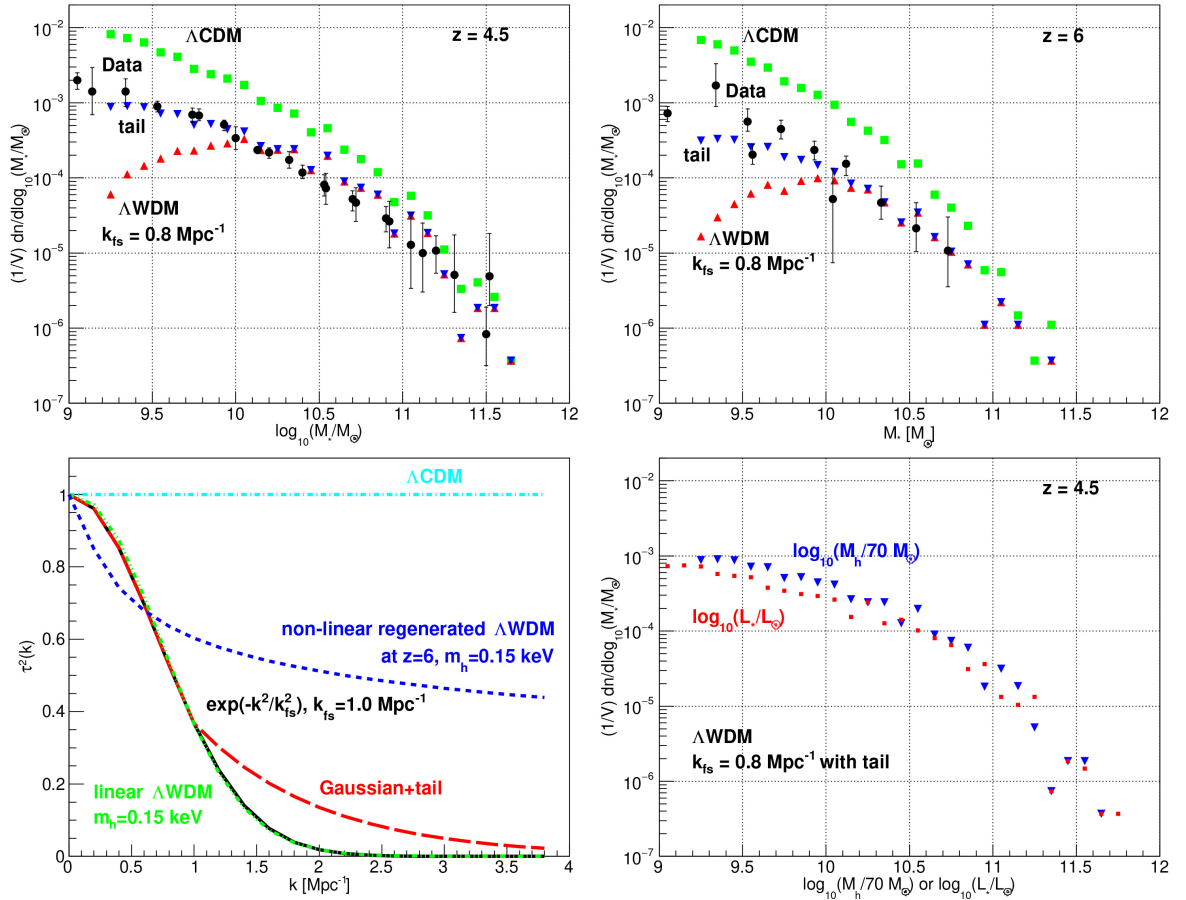


**Figure 2.** Upper panels: stellar mass distributions, from simulations and data, at  $z = 4.5$  and  $6$ . The simulations correspond to  $\Lambda$ CDM,  $\Lambda$ WDM with Gaussian  $\tau^2(k)$  with  $k_{fs} = 0.8 \text{ Mpc}^{-1}$ , and the same plus a “tail”, see equation (22). For references to the original data points see [13]. Bottom left: warm dark matter cut-off factor  $\tau^2(k)$  with the Gaussian function (2) with  $k_{fs} = 1 \text{ Mpc}^{-1}$ , the Gaussian+tail of Equation (22), the “linear”  $\tau^2(k)$  from [4], and the “non-linear” regenerated  $\tau^2(k)$  from [25] with  $m_h = 0.15 \text{ keV}$  and  $z = 6$ . The Gaussian and “linear” curves overlap in this figure. Bottom right: comparison of distributions of halo mass  $M_h$  and stellar luminosity  $L_*$  of the simulation with  $z = 4.5$ .

simulations of  $\Lambda$ WDM if the Gaussian  $\tau^2(k)$  develops a “tail”. This tail need not be of primordial origin: it may be due to limitations of current galaxy generators. Let us mention that the simulations in [21] and [24] are warm dark matter only, they do not include baryons, and baryons act as a cold “tail”. The needed extra tail is much smaller than the tail that current generators already obtain [5] [25]. The simulations in [24] include proto-galaxies, and go a long way between simulations in [21] (similar to the Press-Schechter prediction with a sharp- $k$  window function) and data. In any case, the “tail” needs to be in place by  $z \approx 12$  in order to obtain timely reionization even for  $k_{fs} \approx 1 \text{ Mpc}^{-1}$ , see figure 4 of [27]. To settle this issue, future simulations are needed that have enough resolution to describe the formation of “stripped down” galaxies, and that bridge the gap between the halo mass  $M_h$  and the observable galaxy stellar luminosity  $L_*$ .

## 7. Comments on the Lyman- $\alpha$ Forest

Reionization is beautifully illustrated in [28]. During the dark ages the universe baryonic matter is mostly neutral hydrogen and neutral helium. At about  $z \approx 12$ , first quasars begin ionizing and heating the gas in bubbles expanding away from the quasar. As a result, peaks in the dark matter density correspond to minimums of the neutral hydrogen density. The bubbles overlap at about  $z = 6$ .

Light from quasars is observed to have a “forest” of absorption lines due to Lyman  $1s \leftrightarrow 2p$  transitions (at  $\lambda_\alpha = 1215.67 \text{ \AA}$ ) of intervening clouds of neutral hydrogen [29]. In principle, each line obtains the redshift  $z$  of the cloud, the column density of neutral hydrogen  $N_{\text{HI}}$  (typically  $10^{13}$  to  $10^{14} \text{ cm}^{-2}$ ), the thickness of the cloud along the line-of-sight (tens to hundreds of kpc), and (partially degenerate) its temperature (typically  $10^4$  to  $3 \times 10^4 \text{ K}$ ). Simulations of the inter-galactic medium at  $z = 3$  show that the (mostly ionized) baryon density tracks the dark matter density down to the Jeans length where baryon pressure dominates gravity, with a fraction of neutral atomic hydrogen (HI) of order  $10^{-5}$  that depends on temperature  $T$ , and on the ionization rate  $\Gamma$  due to ultra-violet photons.

The inter-galactic dark matter resembles a honey-comb of voids, surrounded by sheets, that meet at filaments, that meet at spheroidal nodes. Most of the Galaxies form in nodes and filaments.

“For a characteristic hydrogen number density of  $55 \text{ m}^{-3}$ , corresponding to 5 times the mean baryon density at  $z = 3$ , and a characteristic temperature of  $2 \times 10^4 \text{ K}$ , the pressure is  $10^6 \text{ K}\cdot\text{m}^{-3}$ , and the baryon Jeans length is 320 kpc” [29]. In comparison, the warm dark matter Jeans length, at  $z = 3$  with  $v_{\text{rms}} = 0.67 \text{ km/s}$ , corresponding to thermal  $m_h \approx 100 \text{ eV}$ , is  $\lambda_{Jh} = 30 \text{ kpc}$ . Filament thicknesses are of order 100 kpc [29].

Let us comment on figure 3 of [30] that presents the Lyman- $\alpha$  relative flux 1-dimensional power spectrum  $\Delta_{\text{F1D}}^2(k_z) \equiv k_z P_{\text{F1D}}(k_z)/\pi$  for  $k_z$  in the range 0.0005 to 0.02 s/km. We consider  $z = 4.4$ , so the measured range of  $k_z$  is 0.05 to  $1.75 \text{ Mpc}^{-1}$  (the conversion factor is  $\approx H_0 \sqrt{\Omega_m (1+z)}$ ). The relation between the 1-dimensional and 3-dimensional flux power spectrum is [29]

$$\frac{\Delta_{\text{F1D}}^2(k_z)}{k_z} = \int_{k_z}^{\infty} \frac{\Delta_F^2(k)}{k^2} dk. \quad (25)$$

where  $\Delta_F^2(k) \equiv k^3 P_F(k)/(2\pi^2)$ . Note that this integral must reach well past the maximum observed  $k_z$  to avoid a drop in  $\Delta_{\text{F1D}}^2(k_z)$ . We select a “bias factor”  $b(k)$  such that  $P_F(k) = b(k)P(k)$  obtains the measured  $\Delta_{\text{F1D}}^2(k_z)$ , where  $P(k)$  is the  $\Lambda$ CDM dark matter comoving linear power spectrum [2]. Agreement is obtained with  $b(k) = 0.016$  independent of  $k$ , so flux fluctuations  $\delta_F = (F - \langle F \rangle)/\langle F \rangle$  appear to track the dark matter density fluctuations, at least in low density regions of the universe, *i.e.* away from nodes. Multiplying  $P_F(k)$  by the linear cut-off factor  $\tau^2(k)$  obtained from [4] rules out  $m_h = 0.1 \text{ keV}$  if

non-linear regeneration of small scale structure is neglected, which is not justified [5]. If instead of the linear cut-off factor  $\tau^2(k)$  from [4], we take the non-linear regenerated cut-off factor of [25], then we find that  $m_h = 0.1$  keV is allowed!

Now consider figure 11 of [25] that presents the Lyman- $\alpha$  1-dimensional power spectrum  $\Delta_{F1D}^2(k_z)$  for  $k_z$  in the range 0.0013 to 0.08 s/km, see **Figure 3**. We consider  $z = 5.4$ , so the range of  $k_z$  is 0.12 to 7.6 Mpc $^{-1}$ . In this case, for  $\Lambda$ CDM, we obtain a bias factor  $b(k) = 0.06$  independent of  $k$  that obtains the measured  $\Delta_{F1D}^2(k_z)$  for  $k_z < 0.025$  s/km. For  $k_z > 0.04$  s/km, the measured  $\Delta_{F1D}^2(k_z)$  drops below the values obtained from  $P_F(k) = 0.06P(k)$ . As an exercise, let us assume that this drop is due to warm dark matter free-streaming. Again we take the linear cut-off factor  $\tau^2(k)$  from [4]. Then we obtain  $m_h = 2.2 \pm 0.4$  (stat) keV, and  $b = 0.08 \pm 0.01$ , with  $\chi^2 = 2.9$  for 8 degrees of freedom, if we neglect non-linear regeneration of small scale structure. In this case  $m_h = 0.1$  keV is excluded with  $\chi^2 = 295$  for 9 degrees of freedom, see **Figure 3**. If instead of the linear cut-off factor  $\tau^2(k)$  from [4], we take the non-linear regenerated cut-off factor of [25], we obtain the measurement  $m_h = 0.50 \pm 0.21$  (stat) keV, and  $b = 0.08 \pm 0.01$ , with  $\chi^2 = 8.8$  for 8 degrees of freedom. Fixing  $m_h = 0.1$  keV obtains  $b = 0.15 \pm 0.01$  and  $\chi^2 = 11.7$  for 9 degrees of freedom (with statistical uncertainties only), so  $m_h = 0.1$  keV is not ruled out! For the  $\Lambda$ CDM model we obtain  $b = 0.054 \pm 0.003$  and  $\chi^2 = 27.8$  for 9 degrees of freedom. See **Figure 3**. The results of this section are in line with pioneering studies in [5].

Question: Why does  $\Delta_{F1D}^2(k_z)$  in [25] or [30] decrease with decreasing  $z$ , while the proper dark matter density power spectrum has the opposite behaviour?

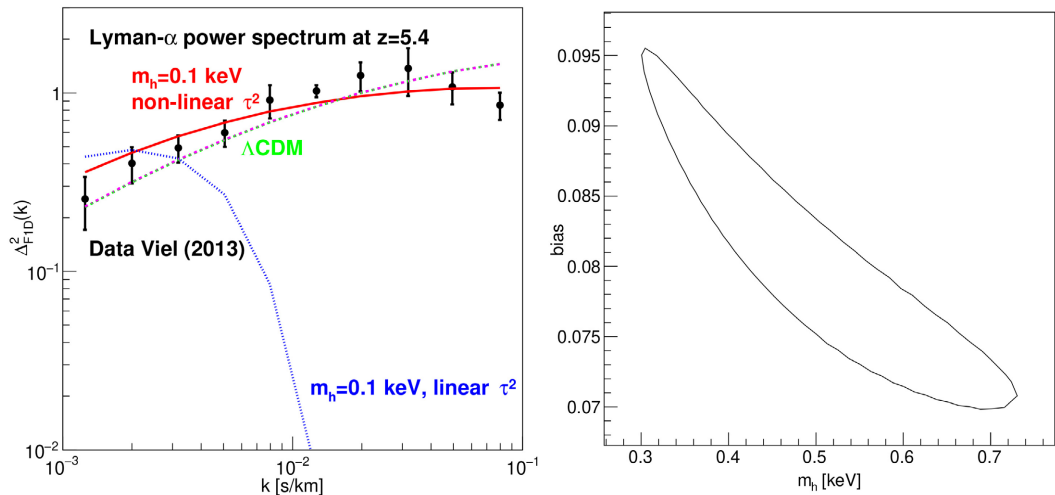


**Figure 3.** Left: Measured Lyman- $\alpha$  forest power spectrum at  $z = 5.4$  from figure 11 of [25], compared with  $\Lambda$ CDM, and with  $\Lambda$ WDM with  $m_h = 0.1$  keV, and linear [4] or non-linear [25] cut-off factors  $\tau^2(k)$ . Right: 1-standard deviation contour in the  $(m_h, b)$  plane assuming the non-linear cut-off factor  $\tau^2(k)$  [25], see text.

## 8. Conclusions

A detailed no freeze-in and no freeze-out warm dark matter scenario has emerged from fits to approximately 60 relaxed spiral galaxy rotation curves, and from measurements of galaxy stellar mass distributions. The resulting thermal relic dark matter mass is of order  $m_h \approx 100$  eV, depending on the spin and decoupling temperature of the dark matter particles, see **Table 1**. Numerous studies have ruled out such a low thermal relic mass  $m_h$ . These studies may well be correct, in which case we need to understand why the measured dispersion velocity  $v_{\text{rms}}(1)$  is approximately the same for all studied relaxed galaxies, why the *measured*  $v_{\text{rms}}(1) = 0.79 \pm 0.33$  (stat) km/s and  $k_{\text{fs}} = 0.90^{+0.44}_{-0.40}$  Mpc<sup>-1</sup> each happen to coincide with the no freeze-in and no freeze-out scenario, why the free-streaming mass  $M_{\text{fs}} = 9 \times 10^{11} M_{\odot}$  (from (21) with  $k_{\text{fs}}$ ) is of Galactic mass, and hence addresses the missing satellite issue, and why  $k_{\text{fs}} \approx 1$  Mpc<sup>-1</sup> happens to be the warmest dark matter that may be consistent with reionization.

It is significant that the Particle Data Group quotes lower limits to the dark matter particle mass of 70 eV for fermions, and  $10^{-22}$  eV for bosons [1]. It is also interesting to note that the onset of degeneracy spoils the fits to spiral galaxy rotation curves, obtaining lower limits of 48 eV for fermions, see figure 5 of [13], and 45 eV for bosons [9]. We find that different treatments of the non-linear regeneration of small scale structure, within current uncertainties, may change a *measurement* of  $m_h$  into a *limit*, and vice versa, see **Figures 1-3**. The core of galaxies is (arguably) evidence that dark matter is warm [8]. New studies, with data and simulations, are needed to better understand the warm dark matter tail. These simulations need to have sufficient resolution to reliably generate “stripped down” galaxies, and need to include the baryon physics to obtain the observable stellar luminosity  $L_*$ , as well as first stars to understand reionization.

## Conflicts of Interest

The author declares no conflicts of interest regarding the publication of this paper.

## References

- [1] Zyla, P.A., *et al.* (2020) The Review of Particle Physics. *Progress of Theoretical and Experimental Physics*, **2020**, 083C01.
- [2] Weinberg, S. (2008) *Cosmology*. Oxford University Press, Oxford.
- [3] Boyanovsky, D., de Vega, H.J. and Sanchez, N.G. (2008) The Dark Matter Transfer Function: Free Streaming, Particle Statistics and Memory of Gravitational Clustering. *Physical Review D*, **78**, Article ID: 063546. <https://doi.org/10.1103/PhysRevD.78.063546>
- [4] Viel, M., Lesgourgues, J., Haehnelt, M.G., Matarrese, S. and Riotto, A. (2005) Constraining Warm Dark Matter Candidates Including Sterile Neutrinos and Light Gravitinos with WMAP and the Lyman- $\alpha$  Forest. *Physical Review D*, **71**, Article ID: 063534. <https://doi.org/10.1103/PhysRevD.71.063534>
- [5] White, M. and Croft, A.A.C. (2018) Suppressing Linear Power on Dwarf Galaxy

- Halo Scales. *The Astrophysical Journal*, **539**, 497-504.  
<https://doi.org/10.1086/309273>
- [6] Hoeneisen, B. (2019) Simulations and Measurements of Warm Dark Matter Free-Streaming and Mass. *International Journal of Astronomy and Astrophysics*, **9**, 368-392. <https://doi.org/10.4236/ijaa.2019.94026>
- [7] Smith, R.E. and Markovič, K. (2011) Testing the Warm Dark Matter Paradigm with Large-Scale Structures. *Physical Review D*, **84**, Article ID: 063507.  
<https://doi.org/10.1103/PhysRevD.84.063507>
- [8] Hoeneisen, B. (2021) A Study of Three Galaxy Types, Galaxy Formation, and Warm Dark Matter. *International Journal of Astronomy and Astrophysics*, **11**, 489-508.  
<https://doi.org/10.4236/ijaa.2021.114026>
- [9] Hoeneisen, B. (2019) A Study of Dark Matter with Spiral Galaxy Rotation Curves. *International Journal of Astronomy and Astrophysics*, **9**, 71-96.  
<https://doi.org/10.4236/ijaa.2019.92007>
- [10] de Blok, W.J.G., *et al.* (2008) High-Resolution Rotation Curves and Galaxy Mass Models from THINGS. *The Astronomical Journal*, **136**, 2648.  
<https://doi.org/10.1088/0004-6256/136/6/2648>
- [11] Lelli, F., McGaugh, S.S. and Schombert, J.M. (2016) SPARC: Mass Models for 175 Disk Galaxies with Spitzer Photometry and Accurate Rotation Curves. *The Astronomical Journal*, **152**, 157. <https://doi.org/10.3847/0004-6256/152/6/157>
- [12] Hoeneisen, B. (2019) The Adiabatic Invariant of Dark Matter in Spiral Galaxies. *International Journal of Astronomy and Astrophysics*, **9**, 355-367.
- [13] Hoeneisen, B. (2020) Fermion or Boson Dark Matter? *International Journal of Astronomy and Astrophysics*, **10**, 203-223. <https://doi.org/10.4236/ijaa.2020.103011>
- [14] Paduroiu, S., Revaz, Y. and Pfnegger, D. (2015) Structure Formation in Warm Dark Matter Cosmologies Top-Bottom Upside-Down.  
<https://arxiv.org/pdf/1506.03789.pdf>
- [15] Hoeneisen, B. (2021) Adding Dark Matter to the Standard Model. *International Journal of Astronomy and Astrophysics*, **11**, 59-72.  
<https://doi.org/10.4236/ijaa.2021.111004>
- [16] Hoeneisen, B. (2000) A Simple Model of the Hierarchical Formation of Galaxies. arXiv: astro-ph/0009071.
- [17] Hoeneisen, B. (2018) Study of Galaxy Distributions with SDSS DR14 Data and Measurement of Neutrino Masses. *International Journal of Astronomy and Astrophysics*, **8**, 230-257. <https://doi.org/10.4236/ijaa.2018.83017>
- [18] Press, W.H. and Schechter, P. (1974) Formation of Galaxies and Clusters of Galaxies by Self-Similar Gravitational Condensation. *The Astrophysical Journal*, **187**, 425-438. <https://doi.org/10.1086/152650>
- [19] Sheth, R.K. and Tormen, G. (1999) Large-Scale Bias and the Peak Background Split. *Monthly Notices of the Royal Astronomical Society*, **308**, 119-126.  
<https://doi.org/10.1046/j.1365-8711.1999.02692.x>
- [20] Sheth, R.K., Mo, H.J. and Tormen, G. (2001) Ellipsoidal Collapse and an Improved Model for the Number and Spatial Distribution of Dark Matter Haloes. *Monthly Notices of the Royal Astronomical Society*, **323**, 1-12.  
<https://doi.org/10.1046/j.1365-8711.2001.04006.x>
- [21] Schneider, A., Smith, R.E. and Reed, D. (2013) Halo Mass Function and the Free Streaming Scale. *MNRAS*, **433**, 1573-1587. <https://doi.org/10.1093/mnras/stt829>
- [22] Schneider, A. (2015) Structure Formation with Suppressed Small-Scale Perturba-

- tions. *MNRAS*, **451**, 3117-3130. <https://doi.org/10.1093/mnras/stv1169>
- [23] Hoeneisen, B. (2020) Cold or Warm Dark Matter? A Study of Galaxy Stellar Mass Distributions. *International Journal of Astronomy and Astrophysics*, **10**, 57-70. <https://doi.org/10.4236/ijaa.2020.102005>
- [24] Angulo, R.E., Hahn, O. and Abel, T. (2013) The Warm Dark Matter Halo Mass Function below the Cut-Off Scale. *MNRAS*, **434**, 3337. <https://doi.org/10.1093/mnras/stt1246>
- [25] Markovič and Viel, M. (2013) Lyman- $\alpha$  Forest and Cosmic Weak Lensing in a Warm Dark Matter Universe. Cambridge University Press, Cambridge. <https://doi.org/10.1017/pasa.2013.43>
- [26] Binney, J. and Tremaine, S. (2008) Galactic Dynamics. 2nd Edition, Princeton University Press, Princeton. <https://doi.org/10.1515/9781400828722>
- [27] Lapi, A. and Danese, L. (2015) Cold or Warm? Constraining Dark Matter with Primeval Galaxies and Cosmic Reionization after Planck. *Journal of Cosmology and Astroparticle Physics*, **9**, 3. <https://doi.org/10.1088/1475-7516/2015/09/003>
- [28] Chardin, J., Puchwein, E. and Haehnelt, M.G. (2017) Large Scale Opacity Fluctuations in the Ly $\alpha$  Forest: Evidence for QSOs Dominating the Ionizing UV Background at  $z \approx 5.56$ ? *MNRAS*, **465**, 3429. <https://doi.org/10.1093/mnras/stw2943>
- [29] Meiksin, A.A. (2009) The Physics of the Intergalactic Medium. *Reviews of Modern Physics*, **81**, 1405-1469. <https://doi.org/10.1103/RevModPhys.81.1405>
- [30] Baur, J., Palanque-Delabrouille, N., Yèche, N., Magneville, C. and Viel, M. (2016) Lyman-alpha Forests Cool Warm Dark Matter. *Journal of Cosmology and Astroparticle Physics*, **8**, 12. <https://doi.org/10.1088/1475-7516/2016/08/012>